American Journal of Electrical Power and Energy Systems
2026, Vol. 15, No. 2, pp. 27–33
https://doi.org/10.11648/j.epes.20261502.12

Research Article

Fabrication of Amorphous Carbon-Coated Co_3O_4 (Co_3O_4@C) Composite and Its Enhanced Electrochemical Performance for Supercapacitor Electrodes

Xiaochen Sun[1, *], Chaocao Cao[1], Limin Zhao[1, 2], Caixia Song[1], Dan Sun[1]

[1]School of Energy and Electric Power Engineering, Xinjiang Vocational University of Technology, Urumqi, China

[2]School of Emergency Management, Lanzhou Resource and Environment Vocational and Technical University, Lanzhou, China

Abstract

In this work, Co_3O_4@C composite electrode materials were successfully fabricated by coating amorphous carbon on Co_3O_4 nanorods. Electrochemical tests demonstrated that the Co_3O_4@C composite exhibited superior electrochemical performance compared with pure Co_3O_4, including larger capacitive response, higher specific capacitance, and more excellent rate capability and cycle stability. Specifically, the Co_3O_4@C composite delivered specific capacitances of 924, 830, 752, and 680 F g^{-1} at current densities of 2, 5, 8, and 10 A g^{-1}, respectively, retaining 73.6% of its initial capacitance when the current density was increased from 2 to 10 A g^{-1}. After 2000 consecutive charge–discharge cycles, the capacitance retention of Co_3O_4@C reached 89.4%, which was higher than that of pure Co_3O_4 (85.3%). Moreover, the Co_3O_4@C composite possessed accelerated ion and electron transport kinetics compared with pure Co_3O_4. The enhanced electrochemical performance of Co_3O_4@C can be ascribed to the synergistic effect between Co_3O_4 and amorphous carbon, the improved electrical conductivity provided by the carbon component, and the protective role of the carbon layer in mitigating the agglomeration and structural degradation of Co_3O_4 during cycling. These findings suggest that the Co_3O_4@C composite is a promising electrode material for high-performance supercapacitors.

Keywords

Co_3O_4@C Composite, Amorphous Carbon, Supercapacitor, Electrode Material, Electrochemical Performance, Pseudocapacitance

1. Introduction

With the intensification of the global energy crisis and the deep implementation of the "dual-carbon" strategy, the development of efficient, eco-friendly, and low-cost energy storage technologies has become a cutting-edge focus of current scientific research. Lithium-ion batteries and supercapacitors, as the main representatives of electrochemical energy storage devices, are also hotspots in current research [1-7]. Lithium-ion batteries are widely used in various fields owing to their high energy density and fast charge–discharge capability. However, their inherent drawbacks, such as a tendency to cause short circuits, high sensitivity to ambient temperature, and short cycle life, limit

*Correspondence: Xiaochen Sun (1026735340@qq.com)

Received: 6 March 2026; **Accepted:** 18 March 2026; **Published:** 23 April 2026

their application in fast-charging/discharging and high-power output devices [8-13]. In contrast, supercapacitors exhibit numerous advantages, including high power density, fast charge–discharge capability, ultra-long cycle life, high safety, and environmental friendliness, showing broad application prospects in new energy vehicles, smart grids, and other fields [14-16].

Cobalt tetroxide (Co_3O_4) is regarded as a promising and extensively studied electrode material for supercapacitors due to its high theoretical specific capacitance, abundant redox reactivity, environmental friendliness, low cost, and simple preparation methods. In recent years, researchers have developed various Co_3O_4 nanostructures, including nanoparticles, nanofibers, microspheres, nanoboxes, nanocages, hollow spheres, and nanoneedles. Vijayakumar et al. [17] prepared cobalt oxide nanoparticles via a simple microwave method. The maximum specific capacitance obtained from charge–discharge tests was 519 F g^{-1}, and the specific capacitance decreased by only approximately 1.3% after 1000 consecutive charge–discharge cycles.

Duan et al. [18] fabricated microporous Co_3O_4 powder using a low-cost microwave plasma chemical vapor deposition method. After 4000 cycles, the specific capacitance of the etched microporous Co_3O_4 powder reached 128 F g^{-1}, which was 3.5 times that of the pristine powder. Chen et al. [19] developed a Co_3O_4 electrode with a flower-like nanoparticle three-level structure via a hydrothermal method followed by sintering. It exhibited excellent rate capability at current densities ranging from 0.5 to 40 A g^{-1}, with a specific capacitance retention of 98.5% after 2000 charge–discharge cycles.

2. Experimental Section

2.1. Synthesis of Co_3O_4

$Co(NO_3)_2 \cdot 6H_2O$ (0.582 g), NH_4F (0.37 g), and $CO(NH_2)_2$ (0.6 g) were dissolved in 50 mL of deionized water to form a homogeneous solution. The mixture was then transferred into a Teflon-lined autoclave. The autoclave was placed in a reaction oven, gradually heated to 120 ℃, and maintained at this temperature for 5 h. After the reaction, the autoclave was naturally cooled to room temperature. The obtained product was washed several times with anhydrous ethanol and deionized water under ultrasonication to remove surface impurities, followed by drying in a vacuum oven at 60 ℃ for 8 h. Finally, the as-prepared sample was annealed at 450 ℃ for 2 h in air using a horizontal tube furnace.

2.2. Synthesis of Co_3O_4@C

A certain amount of sucrose and an appropriate volume of deionized water were weighed to prepare a 0.1 M sucrose solution. Co_3O_4 obtained from the previous reaction at 120 ℃ for 4 hours was added into the sucrose solution, which was then transferred into a high-pressure autoclave. The autoclave was placed in a reaction chamber and reacted at 180 ℃ for 12 hours. The resulting product was cleaned and dried sequentially. Subsequently, the obtained product was placed into a horizontal tube furnace, heated to 500 ℃ at a heating rate of 5 ℃ min^{-1} under argon atmosphere, and held at this temperature for 2 hours to obtain the Co_3O_4@C composite.

2.3. Materials Characterizations

XRD data of the as-synthesized samples were obtained using an X-ray diffractometer (Bruker D2 PHASER) using Cu Ka radiation (λ = 0.1548 nm). The morphology and atomic content were characterized by eld emission scanning electron microscopy (SEM, ZEISS Sigma 300).

2.4. Electrochemical Measurements

All of the electrochemical measurements, including cyclic voltammetry (CV) tests and galvanostatic charge/discharge (GCD) as well as electrochemical impedance spectroscopy (EIS) were carried out in 2 M KOH aqueous solution on a workstation (Princeton 4000A). A three-electrode conguration was adopted in the experiment, in which Hg/HgO and platinum foil were used as reference and counter electrodes, respectively. The conditions of EIS tests were as follows: alternating current voltage amplitude 5 mV and a frequency ranging from 0.01 to 1×10^5 Hz at open circuit potential.

3. Results and Discussion

Figure 1 shows the XRD pattern of the Co_3O_4@C composite formed by amorphous carbon coating on Co_3O_4. It can be observed from Figure 1 that the pattern clearly indicates the presence of Co_3O_4. The 2θ values at 31.2°, 36.8°, 59.4°, and 65.2 ° correspond to the (220), (311), (511), and (440) crystal planes of Co_3O_4, respectively, which can be attributed to the face-centered cubic (fcc) spinel phase of Co_3O_4 (JCPDS 43-1003). In addition, three strong diffraction peaks corresponding to the Ni foam substrate can also be observed in the pattern. However, no diffraction peaks of the carbon material are detected after carbon coating, which is closely related to the type of coated carbon. Since amorphous carbon is nearly non-crystalline with a very low degree of graphitization and crystallization, and is highly dispersed in the sample, no characteristic peaks appear in the XRD pattern. Nevertheless, its presence can be confirmed by combining other characterization techniques.

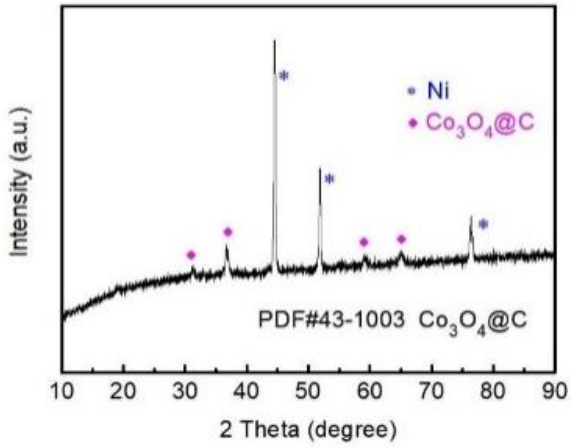

Figure 1. *XRD patterns of as-prepared Co_3O_4@C nanobundles.*

The Co_3O_4 sample was obtained by reaction at 120 ℃ for 4 h, followed by annealing in air. To further investigate the morphology and structure of the Co_3O_4@C composite electrode material, Figure 2 presents SEM images at different magnifications. As observed in Figure 2(a), the sample exhibits a rhombic rod-like structure with regular arrangement. The morphology and size of Co_3O_4@C can be confirmed from the high-magnification SEM image (Figure 2(b)), in which the rhombic rod-like structures of Co_3O_4 are uniformly and densely distributed. The diameter of the nanorods is approximately 300 nm. Owing to the low crystallinity of the amorphous carbon, it shows no fixed morphology or periodic structural regularity.

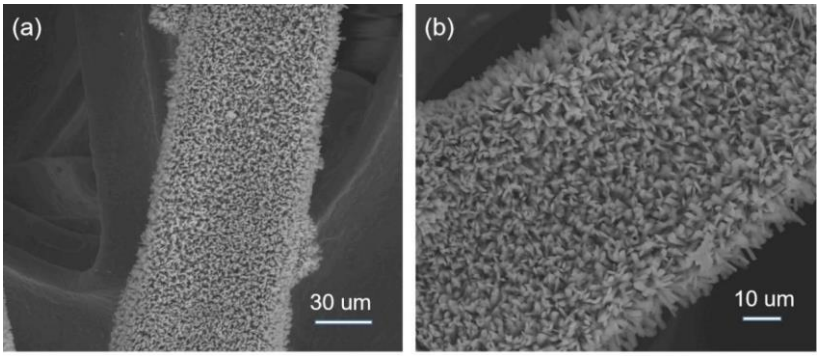

Figure 2. *SEM images of Co_3O_4@C: (a) and (b) different magnified SEM images of Co_3O_4@C nanobundles.*

To further explore the electrochemical performance of cobalt-based materials, cyclic voltammetry (CV) tests were carried out on the electrodes, and the obtained CV curves are shown in Figure 3. The CV curves of Co_3O_4 and Co_3O_4@C were acquired at the same scan rate. By comparing the CV curves of the two electrode materials, it can be observed that the CV curve area of Co_3O_4@C is significantly larger than that of Co_3O_4, as presented in Figure 3(a). This indicates that after carbon coating, Co_3O_4@C exhibits superior capacitive properties. This is not only because a synergistic effect can be formed between Co_3O_4 and the carbon material, but also because the carbon phase contributes a portion of the capacitance. Figure 3(b) displays the CV curves of Co_3O_4@C within a potential window of 0–0.5 V at scan rates ranging from 20 to 60 mV s^{-1}. As the scan rate increases, the area of the CV curves gradually enlarges. Distinct redox peaks appear in the CV profiles, which are quite different from the nearly rectangular shape typical of electric double-layer capacitance. This demonstrates that the measured capacitance is pseudocapacitance, whose behavior is not mainly provided by electrochemical double-layer charging, but primarily originates from redox reactions occurring at the electrode. With increasing scan rate, the redox current density increases accordingly; the anodic peak shifts toward a higher potential, while the cathodic peak moves toward a lower potential. These results clearly prove that the redox process in Co_3O_4@C for capacitive energy storage possesses quasi-reversible characteristics.

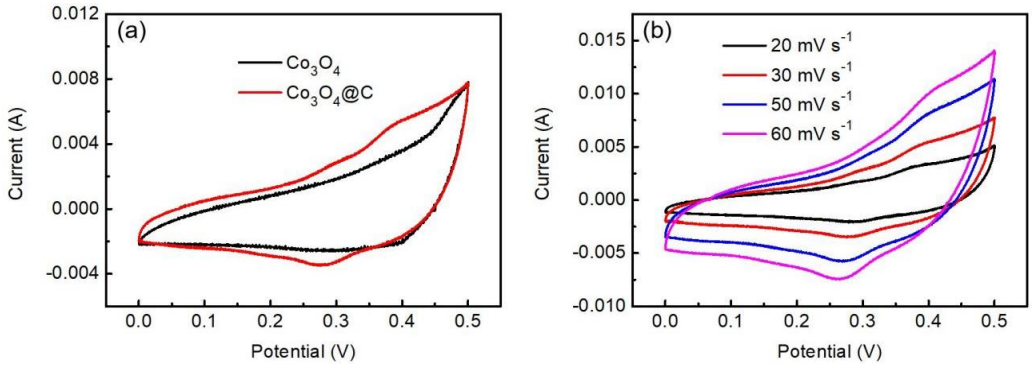

Figure 3. *CV curves of diamond-shaped rod structure Co_3O_4 and Co_3O_4@C: (a) CV curves of Co_3O_4 nanorods and Co_3O_4@C nanorods at at a certain scan rate of 30 mV s^{-1}; (b) CV curves of Co_3O_4@C nanorods at different scan rates (20-60 mV s^{-1}).*

Galvanostatic charge–discharge (GCD) testing is an important technique for evaluating the electrochemical performance of supercapacitors. The GCD curves of the Co_3O_4@C electrode are presented in Figure 4.

At the same current density, the discharge time of the Co_3O_4@C electrode is longer than that of the Co_3O_4 electrode, as shown in Figure 4(a), further demonstrating the excellent charge storage capability of the Co_3O_4@C composite electrode. However, the discharge time of the electrode is not prolonged significantly, resulting in an unobvious improvement in the specific capacitance of the composite material. This is because the theoretical specific capacitance of carbon materials is relatively low, and coating with amorphous carbon cannot obviously enhance the specific capacitance. It can be seen from the charge–discharge curve of Co_3O_4@C in Figure 4(a) that there is a clear distinction below approximately 0.2 V and in the range of 0.2–0.5 V. The potential–time curve below 0.2 V is nearly parallel to the potential axis, revealing electric double-layer capacitive behavior caused by charge separation at the electrode/electrolyte interface. On the other hand, an obvious inclined curve (0.2–0.5 V) appears, representing typical pseudocapacitive characteristics, which may be related to two factors: one is electrochemical adsorption/desorption, and the other is redox reactions occurring at the electrode/electrolyte interface. Figure 4(b) shows the GCD curves of Co_3O_4@C at current densities of 2, 5, 8, and 10 A g^{-1} within a potential window of 0–0.5 V. The capacitance of all samples decreases with increasing discharge current density, which can be attributed to the tortuous diffusion of OH^- ions inside the pores of the electrode material and the electrode resistance. At low discharge current densities, both the inner and outer surfaces of the electrode material contribute to capacitive energy storage. In contrast, at high discharge current densities, ion diffusion during electrochemical reactions only occurs on the outer surface of the electrode material, while reactions on the inner surface are insufficient, leading to a low utilization efficiency of the active material.

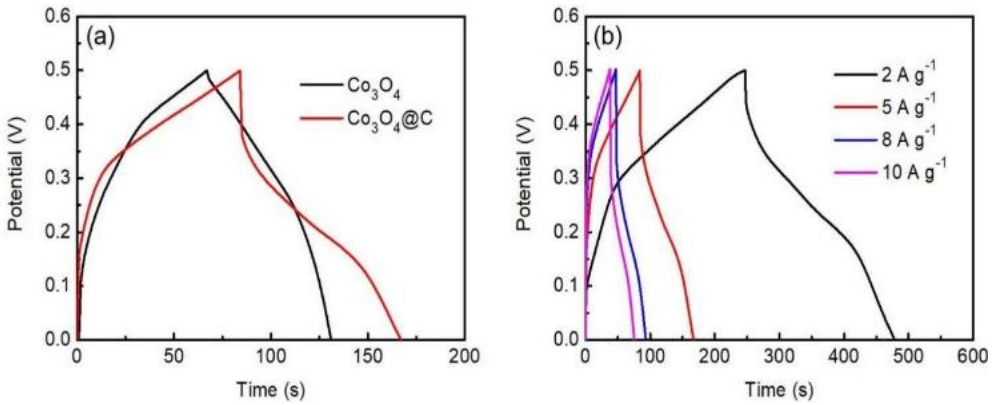

Figure 4. *GCD curves of Co_3O_4 and Co_3O_4@C: (a) at a certain current density of 5 A g^{-1}; (b) GCD curves of Co_3O_4@C at different current densities.*

The rate capability and cycling performance of Co_3O_4@C were further investigated, and the results are displayed in Figure 5. As shown in Figure 5(a), the specific capacitances of the Co_3O_4@C electrode at current densities of 2, 5, 8, and 10 A g^{-1} are 924, 830, 752, and 680 F g^{-1}, respectively. The specific capacitance is maximized at low current densities because OH^- ions migrate more actively on the electrode surface at low current densities, whereas diffusion limitations restrict the movement of OH^-

ions at high current densities, resulting in reduced capacitance. The relatively high content of amorphous carbon in Co_3O_4@C may stabilize Co_3O_4 during charge–discharge cycling. After increasing the current density from 2 A g^{-1} to 10 A g^{-1}, the capacitance retention of Co_3O_4@C is 73.6%. To further verify that Co_3O_4@C can serve as an electrode material for supercapacitors, its cycling stability was tested. As shown in Figure 5(b), after 2000 charge–discharge cycles, Co_3O_4@C still exhibits high capacitive energy storage efficiency, with a capacitance retention of 89.4%, which is higher than that of Co_3O_4 (85.3%). Therefore, the enhanced performance of Co_3O_4@C can be attributed to three factors: the carbon layer coated on the Co_3O_4 surface, which effectively suppresses the agglomeration and degradation of Co_3O_4 during cycling; the synergistic effect between Co_3O_4 and amorphous carbon; and the improved electrical conductivity of the composite due to the high carbon content.

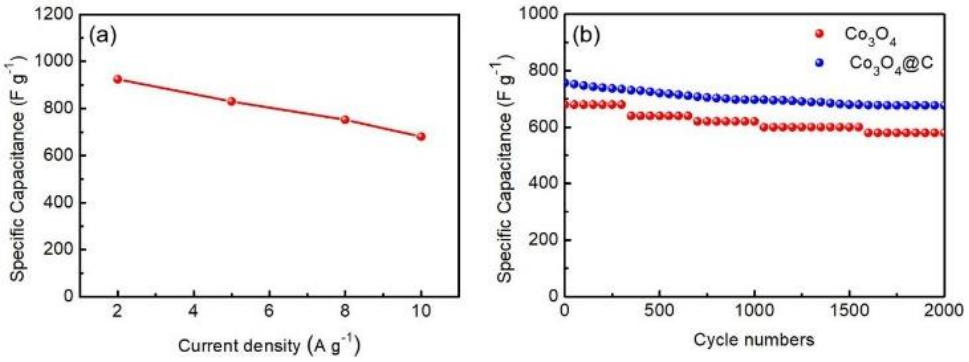

Figure 5. *Electrochemical performance of Co_3O_4 and Co_3O_4@C: (a) Specific capacitances at different current densities of Co_3O_4@C; (b) cycling stability of Co_3O_4 and Co_3O_4@C for 2000 cycles at 8 A g^{-1}.*

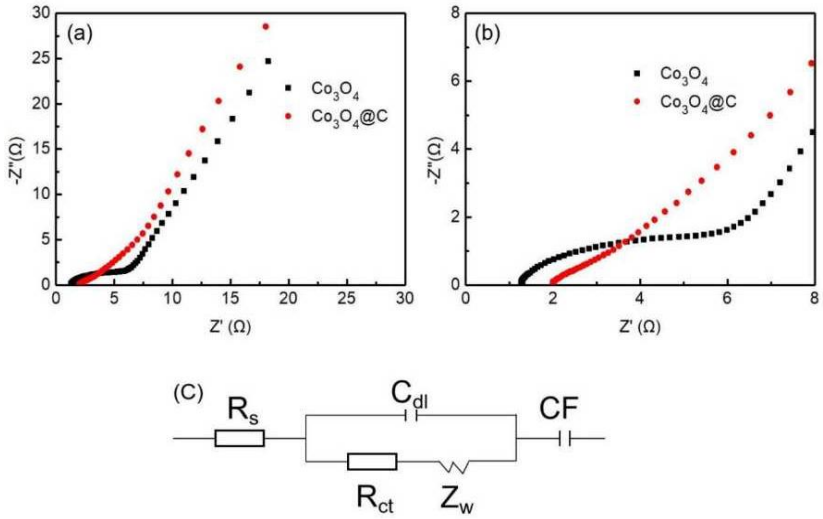

Figure 6. *Electrochemical impedance of Co_3O_4 and Co_3O_4@C: (a) Nyquist plots of Co_3O_4 and Co_3O_4@C; (b) high frequency region Nyquist plots of Co_3O_4 and Co_3O_4@C; (c) the simulated circuit diagram of Co_3O_4@C.*

To further understand the electrochemical characteristics of the Co_3O_4@C electrode material, where high specific capacitance and low resistance are preferred properties for pseudocapacitive electrode materials, electrochemical impedance spectroscopy (EIS) was employed to further characterize the electrochemical performance of the sample. Figure 6(a) shows the Nyquist plot of the Co_3O_4@C electrode. The intercept of the semicircle in the high-frequency region on the Z'-axis represents the internal resistance Rs. The diameter of the semicircle in the high-frequency region corresponds to the charge-transfer resistance Rct, which is related to the electroactive surface area of the electrode; the diameter of the semicircle reflects the magnitude of Rct. As observed in Figure 6(b), the semicircle diameter of the Co_3O_4@C electrode in the high-frequency region is smaller than that of pure Co_3O_4, indicating that Co_3O_4@C possesses a lower Rct value. This charge-transfer resistance is associated with the Faradaic redox reactions of the Co_3O_4 electrode material, which involve the exchange of OH^- ions. After carbon coating, the charge-transfer rate is accelerated, leading to a significant

improvement in electrochemical performance. Figure 6(c) presents the equivalent circuit model employed for fitting the EIS data of Co_3O_4@C. The fitted values of Rs and Rct are determined to be 0.51 Ω and 1.55 Ω for Co_3O_4@C, respectively, whereas those of pure Co_3O_4 are 1.23 Ω and 2.58 Ω. The lower Rs value of the Co_3O_4C electrode originates from the intrinsic resistance of the electrode material and its interfacial contact with the electrolyte. Meanwhile, the significantly reduced Rct value of Co_3O_4@C is mainly attributed to the strong interfacial interaction between amorphous carbon and Co_3O_4 nanobundles, which effectively accelerates interfacial charge transfer and improves the overall electronic conductivity of the electrode.

4. Conclusion

In summary, amorphous carbon-coated Co_3O_4 (Co_3O_4@C) composite electrode materials were successfully synthesized and comprehensively characterized. Structural and morphological analyses confirmed the formation of pure spinel-phase Co_3O_4 with a regular rhombic rod-like structure, while the coated carbon existed in an amorphous state. Electrochemical investigations demonstrated that the introduction of amorphous carbon effectively enhanced the capacitive performance of Co_3O_4. Compared with pure Co_3O_4, the Co_3O_4@C composite exhibited larger CV curve areas, longer discharge durations, higher specific capacitance, superior rate capability, and improved cycling stability. Notably, the Co_3O_4@C composite maintained a high capacitance retention of 89.4% after 2000 charge–discharge cycles and displayed excellent rate performance with a capacitance retention of 73.6% as the current density increased from 2 to 10 A g^{-1}. EIS results further confirmed that the carbon coating significantly reduced the charge-transfer resistance and improved the electrical conductivity of the composite. The enhanced electrochemical properties of Co_3O_4@C are primarily attributed to three factors: the synergistic interaction between Co_3O_4 and amorphous carbon, the improved electrical conductivity provided by the carbon component, and the protective effect of the carbon layer against the agglomeration and structural collapse of Co_3O_4 during repeated charge–discharge processes. This study demonstrates that the Co_3O_4@C composite possesses excellent electrochemical performance and holds great potential as an advanced electrode material for supercapacitor applications.

Abbreviations

Co_3O_4	Cobalt Tetroxide
XRD	X-ray Diffractometer
SEM	Scanning Electron Microscopy
CV	Cyclic Voltammetry
GCD	Galvanostatic Charge/Discharge
EIS	Electrochemical Impedance Spectroscopy

Author Contributions

Xiaochen Sun: Conceptualization, Resources, Methodology, Writing – original draft, Writing – review & editing
Chaocao Cao: Data curation, Investigation
Limin Zhao: Formal Analysis
Caixia Song: Validation
Dan Sun: Visualization

Conflicts of Interest

There are no conflicts to declare.

References

[1] Zhang L L, Zhao X S. Carbon-based materials as supercapacitor electrodes [J]. Chemical Society Reviews, 2009, 38(9): 2520-2531. https://doi.org/10.1039/b813846j

[2] Chmiola J, Yushin G, Gogotsi Y, et al. Anomalous increase in carbon capacitance at pore sizes less than 1 nanometer [J]. Science, 2006, 313(5794): 1760-1763. https://doi.org/10.1126/science.1132195

[3] Wang G, Zhang L, Zhang J. A review of electrode materials for electrochemical supercapacitors [J]. Chemical Society Reviews, 2012, 41(2): 797-828. https://doi.org/10.1007/s11431-015-5931-z

[4] Wang X, Hu A, Meng C, et al. Recent Advance in Co_3O_4 and Co_3O_4 -Containing Electrode Materials for High-Performance Supercapacitors [J]. Materials, 2020, 25(2): 269. https://doi.org/10.3390/molecules25020269

[5] Jiang Y, Chen L, Zhang H, et al. Two-dimensional Co_3O_4 thin sheets assembled by 3D interconnected nanoflake array framework structures with enhanced supercapacitor performance derived from coordination complexes [J]. Chemical Engineering Journal, 2016, 292: 1-12. https://doi.org/10.1016/j.cej.2016.02.009

[6] Qi F Y, Lu X Y, Wang Y Q, et al. Fabrication of hierarchical MoO_3@$Ni_xCo_{2x}(OH)_{6x}$ core–shell arrays on carbon cloth as enhanced-performance electrodes for asymmetric supercapacitors [J]. Journal of Colloid and Interface Science, 2022, 607, 1253-1261. https://doi.org/10.1016/j.jcis.2021.09.046

[7] Li H, Qi F Y, Yang F, et al. Novel synthesis of hierarchical $NiGa_2O_4$@MnO_2 core-shell hetero-nanostructured nanowall arrays on carbon cloth for high-performance all-solid-state asymmetrical supercapacitors [J]. Journal of Colloid and Interface Science, 2021, 587, 302-310. https://doi.org/10.1016/j.jcis.2020.11.078

[8] Li J, Cheng X, Shashurin A, et al. Review of Electrochemical Capacitors Based on Carbon Nanotubes and Graphene [J]. Graphene, 2012, 1(1): 1-13. https://doi.org/10.4236/graphene.2012.11001

[9] Pan H, Li J, Feng Y P. Carbon Nanotubes for Supercapacitor [J]. Nanoscale Research Letters, 2010, 5(3): 654-668. https://doi.org/10.1007/s11671-009-9508-2

[10] Forse A C, Merlet C, Griffin J M, et al. New Perspectives on the Charging Mechanisms of Supercapacitors [J]. Journal of the American Chemical Society, 2016, 138(18): 5731-5744. https://doi.org/10.1021/jacs.6b02115

[11] Qi F Y, Shao L Y, Shi X Y, et al."Carbon quantum dots-glue" enabled high-capacitance and highly stable nickel sulphide nanosheet electrode for supercapacitors [J]. Journal of Colloid and Interface Science, 2021, 601, 669-677. https://doi.org/10.1016/j.jcis.2021.05.099

[12] Qi F Y, Li H, Yang F, et al. Core-shell coaxially structured $NiCo_2S_4$@TiO_2 nanorod arrays as advanced electrode for solid-state asymmetric supercapacitorss [J]. Nanotechnology, 2021, 32(29), 295705. https://doi.org/10.1088/1361-6528/abf693

[13] Li R, Li J, Liu Q, et al. Recent progress on covalent organic frameworks and their composites as electrode materials for supercapacitors [J]. Advanced Composites and Hybrid Materials, 2025, 8(1): 86. https://doi.org/10.1007/s42114-024-01177-x

[14] Yin B S, Zhang S W, Ren Q Q, et al. Elastic soft hydrogel supercapacitor for energy storage [J]. Journal of Materials Chemistry A, 2017, 5(47): 24942-24950. https://doi.org/10.1039/C7TA08152A

[15] Song X S, Li X F, Bai Z M, et al. Rationally-designed configuration of directly-coated Ni3S2/Ni electrode by RGO providing superior sodium storage [J]. Carbon, 2018, 133: 14-22. https://doi.org/14-22.10.1016/j.carbon.2018.02.101

[16] Lang J, Zhang X, Liu L, et al. Highly enhanced energy density of supercapacitors at extremely low temperatures [J]. Journal of Power Sources, 2019, 423: 271-279. https://doi.org/10.1016/j.jpowsour.2019.03.096

[17] Vijayakumar S, Ponnalagi A K, Nagamuthu S, et al. Microwave assisted synthesis of Co_3O_4 nanoparticles for high-performance supercapacitors [J]. Electrochimica Acta, 2013, 106: 500-505. https://doi.org/10.1016/j.electacta.2013.05.121

[18] Duan Y, Hu T, Yang L, et al. Facile fabrication of electroactive microporous Co_3O_4 through microwave plasma etching for supercapacitors [J]. Journal of Alloys and Compounds, 2019, 771: 156-161. https://doi.org/10.1016/j.jallcom.2018.08.204

[19] Chen J, Xu Z, Zhu H, et al. An ultrafast supercapacitor built by Co_3O_4 with tertiary hierarchical architecture [J]. Vacuum, 2020, 174(1): 109219. https://doi.org/10.1016/j.vacuum.2020.109219